## AUTHOR CONTRIBUTIONS

Conceptualization: NN, RAS, BB-S, AE, HPS, SSC; Data Curation: NN, BB-S; Formal Analysis: NN, DJ; Investigation: NN, DJ; Methodology: NN, DJ, AE, SSC; Resources: BB-S, RAS, HPS; Software: NN, DJ; Supervision: BB-S, AE, SSC; Validation: NN, DJ, RAS; Visualization: NN, DJ; Writing - Original Draft Preparation: NN; Writing - Review and Editing: NN, DJ, RAS, BB-S, MJ, AE, HPS, SSC

***Nathasha Naranpanawa[1,*], Dilki Jayasinghe[2], Richard A. Sturm[3], Brigid Betz-Stablein[3], Monika Janda[2], Anders Eriksson[4], H. Peter Soyer[3] and Shekhar S. Chandra[1]***

*[1]School of Information Technology and Electrical Engineering, The University of Queensland, Brisbane, Australia; [2]Centre for Health Services Research, Faculty of Medicine, The University of Queensland, Brisbane, Australia; [3]Frazer Institute, Dermatology Research Centre, The University of Queensland, Brisbane, Australia; and [4]Precision AI, Brisbane, Australia*

*[*]Corresponding author. e-mail: nathasha.naranpanawa@uq.edu.au*

## SUPPLEMENTARY MATERIAL

Supplementary material is linked to the online version of the paper at www.jidonline.org, and at https://doi.org/10.1016/j.jid.2024.04.029.

## REFERENCES

LabelBox Inc.. https://labelbox.com/; 2018. (accessed June 15, 2023).

Cancer Australia. Relative survival by stage at diagnosis (melanoma). https://ncci.canceraustralia.gov.au/outcomes/relative-survival-rate/relative-survival-stage-diagnosis-melanoma; 2019. (accessed September 27, 2023).

Krohn J, Sundal KV, Frøystein T. Topography and clinical features of iris melanoma. BMC Ophthalmol 2022;22:6.

Laino AM, Berry EG, Jagirdar K, Lee KJ, Duffy DL, Soyer HP, et al. Iris pigmented lesions as a marker of cutaneous melanoma risk: an Australian case-control study. Br J Dermatol 2018;178:1119–27.

Naranpanawa DNU, Gu Y, Chandra SS, Betz-Stablein B, Sturm RA, Soyer HP, et al. Slim-YOLO: a simplified object detection model for the detection of pigmented iris freckles as a potential biomarker for cutaneous melanoma. Proceedings of the digital image computing: technqiues and applications (DICTA). Australia: IEEE: Gold Coast; 2021. p. 1–8.

Redmon J, Farhadi A. YOLOv3: an incremental improvement. https://pjreddie.com/media/files/papers/YOLOv3.pdf; 2018. (accessed June 15, 2023).

Schwab C, Mayer C, Zalaudek I, Riedl R, Richtig M, Wackernagel W, et al. Iris freckles a potential biomarker for chronic sun damage. Invest Ophthalmol Vis Sci 2017;58:BIO174–B179.

# Regional Differences in Itch Transmission

*Journal of Investigative Dermatology* (2024) **144,** 2605–2608; doi:10.1016/j.jid.2024.04.010

## TO THE EDITOR

The nervous system allocates disproportional neuronal resources to sensory information critical for an organism's survival and reproduction. The most striking feature of the somatosensory *homunculus* is the enlarged area representing the distal limbs, especially the hairless glabrous skin regions such as the palms of the hands and soles of the feet, to facilitate environmental exploration. Heightened tactile and pain sensitivity in glabrous skin has been well-established (Mancini et al, 2014). However, whether regional differences exist in itch signal processing is not clear. Interestingly, cholestatic pruritus, itching due to reduced or blocked bile flow, is particularly intense in glabrous skin, suggesting sharpened itch sensitivity to endogenous pruritic stimuli in the glabrous skin (Beuers et al, 2014). Our recent study demonstrated that MrgprC11$^{+}$ dorsal root ganglion sensory neurons mediate both hairy and glabrous skin itch (Steele et al, 2021), providing a cellular target to investigate regional differences in itch. This study revealed heightened itch sensitivity in the glabrous skin, supported by the unique axonal branching pattern of itch-sensing neurons.

We generated *MrgprC11$^{ChR2}$* mice and employed an optogenetic approach to test itch sensitivity in different skin locations (Figure 1a–d). Light stimulation of MrgprC11$^{+}$ nerves in trunk hairy skin evoked significant scratching, whereas activation of MrgprC11$^{+}$ nerves in plantar glabrous skin induced strong biting, both of which demonstrate itch sensations. Interestingly, much lower laser power is required to evoke glabrous skin biting, suggesting heightened itch processing for glabrous skin (Figure 1b). To rule out the possibility that different expression levels of channelrhodopsin-2 contribute to different light thresholds, MrgprC11$^{+}$ skin-innervating neurons were retrogradely labeled and collected for qPCR. Comparable expression levels of channelrhodopsin-2 were observed in trunk skin and glabrous skin-innervating neurons (Figure 1e). Consistently, we found that plantar glabrous skin is much more sensitive to Bam8-22, a MrgprC11 agonist, than other skin locations. Although 10 μM of Bam8-22 is enough to evoke robust biting behavior toward glabrous skin, at least 1.5 mM and 0.3 mM of Bam8-22 are required to induce scratching behavior toward thoracic back skin and the nape of the neck skin respectively (Figure 1f and g).

To gain a mechanistic understanding of the cellular basis of regional differences in itch transmission we performed morphological analysis of MrgprC11$^{+}$ nerves. We first quantified PGP 9.5$^{+}$ and MrgprC11$^{+}$ intraepidermal nerve density in different skin locations in *MrgprC11$^{tdTomato}$* mice. Both PGP 9.5$^{+}$ and MrgprC11$^{+}$ intraepidermal nerve densities in paw skin, including hairy and glabrous sides, are significantly lower than those in thoracic trunk skin (Figure 2a and b). This suggests that heightened itch sensitivity is not attributable to an increased density of peripheral nerves.

We next examined MrgprC11$^{+}$ axonal arborizations in the skin and the spinal cord using axonal tracer alkaline phosphatase. CreERT2 in mice generate background recombination in approximately 1% of dorsal root ganglion sensory neurons without tamoxifen treatment (Xing et al, 2021), allowing

*Abbreviations: CreERT2, Cre recombinase-estrogen receptor fusion protein 2; MrgprC11, Mas-related G protein-coupled receptor C11*

*Accepted manuscript published online 10 May 2024; corrected proof published online 12 June 2024*

© 2024 The Authors. Published by Elsevier, Inc. on behalf of the Society for Investigative Dermatology.

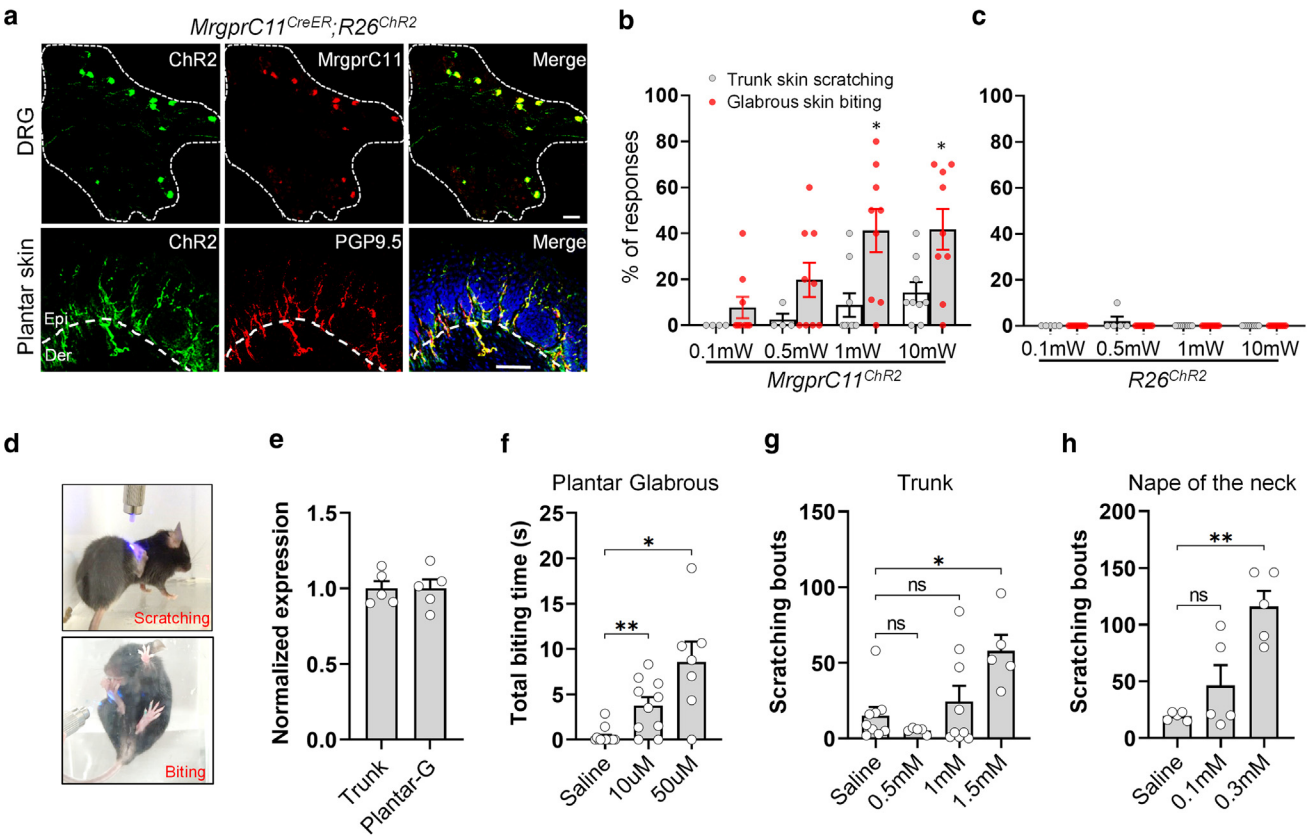


**Figure 1. Higher itch sensitivity of glabrous skin. (A) Generation of *MrgprC11$^{ChR2}$* mice.** (**a**) DRG or hind paw plantar skin sections showing the expression of ChR2(H134R)-EYFP in MrgprC11$^{+}$ neurons and epidermal skin nerves. Epi: epidermis. Der: dermis. Scale bar: 50 μm. (**b**) Percentage of responses induced by different intensities of 473 nm blue light in *MrgprC11$^{ChR2}$* mice. A much lower laser power is required to evoke glabrous skin biting. **(c)** Littermate control *R26$^{ChR2}$* mice did not show any nocifensive behaviors after blue light application. **(d)** Pictures showing the blue light application to the trunk hairy skin (top) or glabrous skin (bottom) of *MrgprC11$^{ChR2}$* mice. (**e**) qPCR analysis showing the expression levels of ChR2 is comparable in glabrous skin-innervating and trunk hairy skin-innervating MrgprC11$^{+}$ neurons. (**f**–**h**) Concentrations of Bam8-22, a MrgprC11 agonist, are required to induce itch behaviors in glabrous skin (**f**), thoracic trunk skin (**g**), and nape of the neck skin (**h**). Data are represented as mean ± SEM. Welch's *t*-test for **b** and **e**. One-way ANOVA for **f**–**h**. $*P < .05$, $**P < .01$. Bam8-22, bovine adrenal medulla 8–22 peptide; ChR2(H134R)-EYFP, chlamydomonas reinhardtii-derived channelrhodopsin-2; DRG, dorsal root ganglion; MrgprC11, Mas-related G protein-coupled receptor C11.

visualization of individual axonal arborizations in the trunk hairy skin (Figure 2c and d) and spinal cord (Supplementary Figure S1). CreERT2 background recombination does not label any glabrous skin-innervating neurons (Xing et al., 2021); therefore, skin arbors in the hind paw glabrous skin were visualized after a low dose of tamoxifen treatment (Figure 2d). MrgprC11$^{+}$ skin arbors in different locations are all typical "free endings" featuring extensive axonal branching inside of the arbor. However, the arbors are larger in the paws and the largest ones are observed in hind paw glabrous skin (Figure 2e). To understand if other subtypes of sensory neurons exhibit similar regional effects, we examined MrgprB4$^{+}$ skin arbors using *MrgprB4$^{PLAP}$* mice. MrgprB4$^{+}$ neurons are C-fiber touch sensors that detect the stroking of hairy skin and do not innervate the glabrous skin (Liu et al, 2007; Vrontou et al, 2013). Interestingly, MrgprB4$^{+}$ arbors exhibit the opposite trend with significantly smaller arbors in the paw skin (Figure 2f). In addition, a previous study showed that MrgprD$^{+}$ sensory neurons, nociceptors mediating pain sensation in glabrous skin, exhibit comparable skin arbor sizes in the trunk and plantar glabrous skin (Olson et al, 2017). These results suggest that different types of skin sensory arbors have distinct regional effects.

We also found that glabrous skin-innervating MrgprC11$^{+}$ neurons exhibit distinct central arbor morphology in the spinal cord. Whole-mount placental alkaline phosphatase histochemistry of the spinal cord isolated from *MrgprC11$^{IAP}$* mice without tamoxifen treatment allowed us to visualize itch-sensing central arbors across the somatotopic map (Supplementary Figure S1). Central projections of sensory neurons are somatotopically organized along the rostrocaudal and mediolateral axis of the spinal cord. MrgprC11$^{+}$ central axons normally turn rostrally after entering the spinal cord, terminate within the segment of entry, and arborize in the superficial dorsal horn (Supplementary Figure S1a–d). Arbors in the spinal regions controlling the trunk (thoracic) and proximal limbs (lateral lumbar) show long morphology with rostrocaudal elongation and mediolateral compression, which is consistent with the previously examined C-type arbors (Sugiura et al, 1993). However, arbors showing round morphology with a much lower Height/Width ratio are observed in regions controlling the distal parts of the body including head/face (upper cervical and medulla), distal limbs (medial cervical

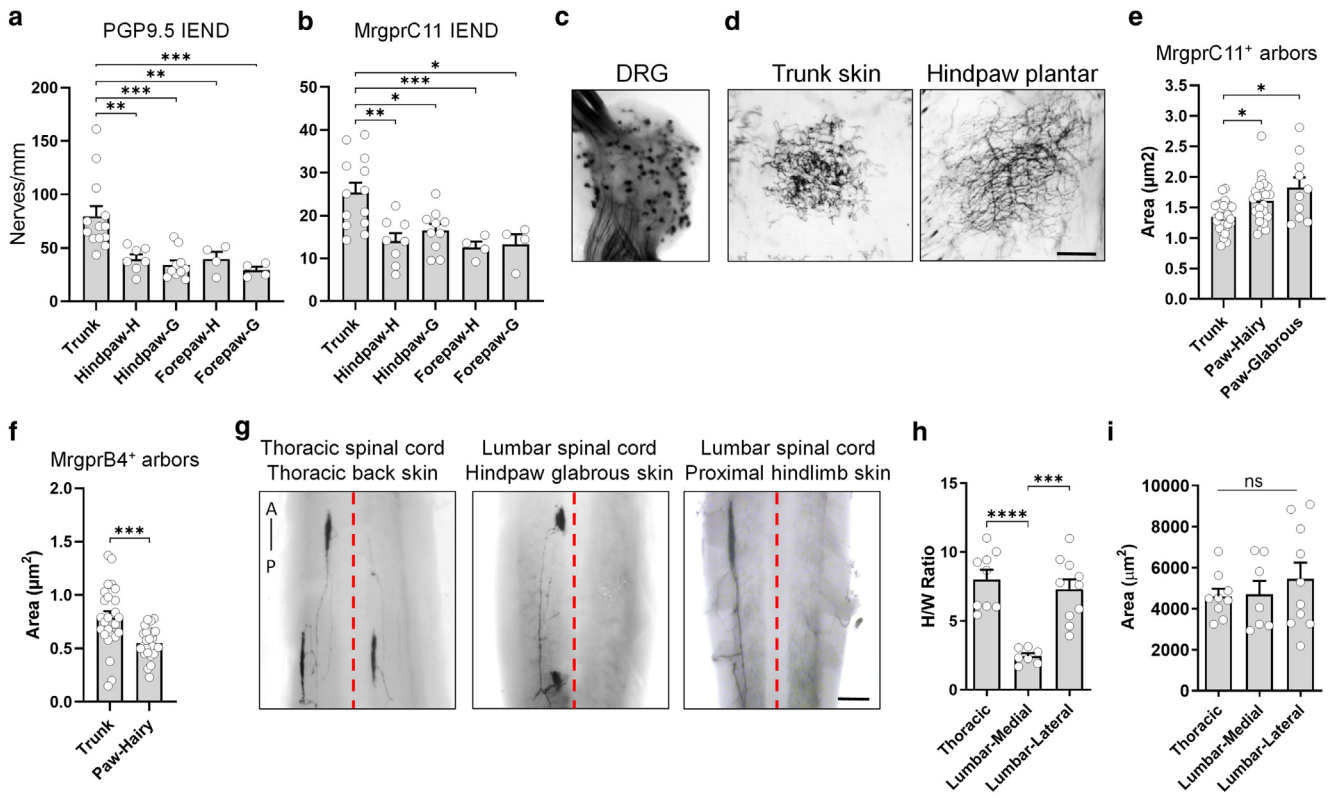


**Figure 2. Regionally distinct morphological organization of itch-sensing arbors in both skin and spinal cord.** (**a**–**b**) PGP 9.5$^+$ (**a**) and MrgprC11$^+$ (**b**) intraepidermal nerve density in different body locations. (**c**) Whole-mount PLAP histochemistry of a lumbar DRG from *MrgprC11*$^{IAP}$ mice without tamoxifen treatment. (**d**) MrgprC11$^+$ arbors in the trunk skin and hind paw plantar glabrous skin. (**e**) MrgprC11$^+$ arbor area in different body locations. (**f**) MrgprB4$^+$ arbor area in different body locations. (**g**) Spinal cord segments from AAV2/1-CMV-FLEX-PLAP injected *MrgprC11*$^{CreER}$ mice showing sparsely labeled MrgprC11$^+$ central arbors. Skin locations injected were indicated. Two or three injections were performed in each skin location to achieve the labeling of at least one DRG neuron. More than one central arbor was observed in some spinal cords. Hind paw glabrous skin-innervating neurons exhibit round arbors in the medial lumbar spinal region. Long arbors were observed when AAV2/1-CMV-FLEX-PLAP was injected into the thoracic back skin or proximal hindlimb skin. (**h**–**i**) Quantification of the Height/Width ratio (**h**) and arbor area (**i**). Data are represented as mean ± SEM. Welch's *t*-test for **f**. One-way ANOVA for other panels. $*P < .05$. $**P < .01$. $***P < .005$. $****P < .001$. ns: not significant. Scale bar in **d** and **g**: 500 μm. A, Anterior; AAV2/1-CMV-FLEX-PLAP, adeno-associated virus serotype 2/1-cytomegalovirus-flip-excision-placental alkaline phosphatase; DRG, dorsal root ganglion; MrgprC11, Mas-related G protein-coupled receptor C11; P, posterior; PGP9.5$^+$, Protein Gene Product 9.5.

and lumbar), tail, and genital area (sacral) (Supplementary Figure S1b–d). Arbors in the sacral region are notably larger, while those in the other segments show similar areas (Supplementary Figure S1g). Since CreERT2 background recombination does not label glabrous skin-innervating neurons, round MrgprC11$^+$ central arbors in the medial lumbar region likely represent neurons innervating the hairy side of the hind paw and ankle area.

To directly correlate central arbor morphologies and the represented skin locations, we injected AAV2/1-CMV-FLEX-PLAP into the skin of *MrgprC11*$^{CreERT2}$ mice. MrgprC11$^+$ central arbors were exclusively observed in spinal segments corresponding to injected skin locations (Figure 2g). Round arbors were observed in medial lumbar segments following injections into the hind paw glabrous skin, whereas long arbors appeared in thoracic and lateral lumbar segments after injections into the thoracic and proximal hindlimb skin respectively (Figure 2g). Round and long arbors share a similar area (Figure 2h and i).

In summary, our results demonstrate regional differences in itch processing, with higher itch sensitivity in glabrous skin, aligning with the regionally distinct morphological organization of itch-sensing neurons. *MrgprC11*$^+$ neurons exhibit low intraepidermal nerve density and larger axonal arborization in glabrous skin, and regionally distinct central arbors in the spinal cord. Previous studies have linked regional-specific central arbor morphology to enhanced signal transmission of touch and pain in glabrous skin (Lehnert et al, 2021; Olson et al, 2017). Conversely, peripheral nerve organization contrasts with higher innervation density and smaller receptive field observed in touch sensors of distal limbs (Brown and Koerber, 1978). Taken together, our findings suggest that region-specific morphological organization serves as a fundamental somatotopic mechanism to facilitate regional differences in sensory processing, although distinct organizations were employed by different sensory modalities.

## DATA AVAILABILITY STATEMENT

All data are included in the manuscript. No large datasets were generated or analyzed during this study.

## ETHICS STATEMENT

All experiments were performed with approval from the Georgia Institute of Technology Animal Use and Care Committee.

**KEYWORDS**
Arborization; Glabrous Skin; Itch; MrgprC11

**ORCIDs**
Yanyan Xing: http://orcid.org/0000-0002-8431-9902
Yeseul Nho: http://orcid.org/0009-0009-9178-8924
Katy Lawson: http://orcid.org/0000-0002-9364-2410
Haley Steele: http://orcid.org/0000-0002-2039-3097
Liang Han: http://orcid.org/0000-0001-8674-6433

**CONFLICT OF INTEREST**
The authors state no conflict of interest.

**ACKNOWLEDGMENTS**
We thank the Department of Animal Resources at Georgia Institute of Technology for the animal care and services. The work was supported by grants from the US National Institutes of Health (HL141269, HL173002) and National Science Foundation (2334697) to LH.

**AUTHOR CONTRIBUTIONS**
Conceptualization: LH; Investigation: YX, YN, KL, HS, LH; Writing - Original Draft: LH; Writing - Review and Editing: YN, KL, LH; Supervision: LH; Funding Acquisition: LH.

***Yanyan Xing*[1], *Yeseul Nho*[1], *Katy Lawson*[1], *Haley Steele*[1] and *Liang Han*[1,*]**

[1]*School of Biological Sciences, Georgia Institute of Technology, Atlanta, Georgia, USA*
[*]*Corresponding author e-mail: lhan41@gatech.edu*

**SUPPLEMENTARY MATERIAL**

Supplementary material is linked to the online version of the paper at www.jidonline.org, and at https://doi.org/10.1016/j.jid.2024.04.010.

**REFERENCES**

Beuers U, Kremer AE, Bolier R, Elferink RP. Pruritus in cholestasis: facts and fiction. Hepatology 2014;60:399–407.

Brown PB, Koerber HR. Cat hindlimb tactile dermatomes determined with single-unit recordings. J Neurophysiol 1978;41:260–7.

Lehnert BP, Santiago C, Huey EL, Emanuel AJ, Renauld S, Africawala N, et al. Mechanoreceptor synapses in the brainstem shape the central representation of touch. Cell 2021;184:5608–5621.e18.

Liu Q, Vrontou S, Rice FL, Zylka MJ, Dong X, Anderson DJ. Molecular genetic visualization of a rare subset of unmyelinated sensory neurons that may detect gentle touch. Nat Neurosci 2007;10:946–8.

Mancini F, Bauleo A, Cole J, Lui F, Porro CA, Haggard P, et al. Whole-body mapping of spatial acuity for pain and touch. Ann Neurol 2014;75:917–24.

Olson W, Abdus-Saboor I, Cui L, Burdge J, Raabe T, Ma M, et al. Sparse genetic tracing reveals regionally specific functional organization of mammalian nociceptors. eLife 2017;6:e29507.

Steele HR, Xing Y, Zhu Y, Hilley HB, Lawson K, Nho Y, et al. MrgprC11$^{+}$ sensory neurons mediate glabrous skin itch. Proc Natl Acad Sci U S A 2021;118:e2022874118.

Sugiura Y, Terui N, Hosoya Y, Tonosaki Y, Nishiyama K, Honda T. Quantitative analysis of central terminal projections of visceral and somatic unmyelinated (C) primary afferent fibers in the guinea pig. J Comp Neurol 1993;332:315–25.

Vrontou S, Wong AM, Rau KK, Koerber HR, Anderson DJ. Genetic identification of C fibres that detect massage-like stroking of hairy skin in vivo. Nature 2013;493:669–73.

Xing Y, Steele HR, Hilley HB, Zhu Y, Lawson K, Niehoff T, et al. Visualizing the itch-sensing skin arbors. J Invest Dermatol 2021;141:1308–16.

## SUPPLEMENTARY MATERIALS AND METHODS

### Mice and Tamoxifen Treatment

All experiments were performed with approval from the Georgia Institute of Technology Animal Use and Care Committee. BAC transgenic line *MrgprC11*$^{CreERT2}$ was generated by a previous study (Xing et al, 2021). The *MrgprB4*$^{PLAP}$ line (Liu et al, 2007) was provided by Dr Xinzhong Dong at Johns Hopkins University. Mice listed below were purchased from Jackson Laboratory: wild-type C57BL/6 mice (Stock No: 000664), *ROSA26*$^{tdTomato}$ (Stock No: 007909), and *ROSA26*$^{IAP}$ (Stock No: 009253), *ROSA26*$^{ChR2\text{-}H134R\text{-}EYFP}$ mice (Stock No: 024109, Ai32). Mice were housed in a vivarium with a 12-hour light/dark cycle, housing groups of 5 maximum, and food/water *ad libitum*. To label MrgprC11$^{+}$ neurons with Cre-dependent reporters tdTomato and ChR2, the mice were treated daily via oral gavage (22 g × 25 mm, FTP-22-25, Instech Laboratories) with 100 mg/kg of tamoxifen (T5648, Sigma) dissolved in sunflower seed oil (S5007, Sigma) for 5 days at 3–4 weeks of age. The CreERT2 in *MrgprC11*$^{CreERT2}$ mice generates background recombination in approximately 1% of dorsal root ganglion sensory neurons without any tamoxifen treatment (Xing et al, 2021). Sparsely labeled MrgprC11$^{+}$ arbors in the spinal cord and trunk skin were visualized using *MrgprC11*$^{IAP}$ mice without tamoxifen treatment. The background recombination of *MrgprC11*$^{CreERT2}$ mice does not label glabrous skin-innervating MrgprC11$^{+}$ neurons. Sparsely labeled MrgprC11$^{+}$ arbors in the glabrous skin were visualized using *MrgprC11*$^{IAP}$ mice treated with low-dose tamoxifen once (0.5 mg/kg, oral gavage).

### Skin Injection of Adeno-Associated Virus

To visualize the central arbors of glabrous skin-innervating MrgprC11$^{+}$ neurons, AAV2/1-CMV-FLEX-PLAP (Addgene 80422, packaged at Emory University Vector Core, titer = 2E+12) was injected into the hind paw plantar glabrous skin, proximal hindlimb skin, or thoracic back skin of *MrgprC11*$^{CreERT2}$ mice using beveled glass capillary needles. Two or 3 injections were performed in each skin location to achieve the labeling of at least one dorsal root ganglion neuron. Mice were treated with tamoxifen (100 mg/kg, intraperitoneally, once daily for 5 days) to activate CreERT2 5 days after the skin injection, and PLAP whole mount histochemistry staining was performed 6 weeks after the skin injection.

### Placental Alkaline Phosphatase (PLAP) Whole Mount Histochemistry Staining

The procedure was performed as previously described (Xing et al, 2021). Briefly, adult mice (8–12 weeks old) were transcardially perfused with ice-cold 4% formaldehyde. To visualize skin arbors, hair removal, and tape stripping were performed to remove the stratum corneum before the perfusion. Tissues were dissected and postfixed in 4% formaldehyde on ice (30 minutes for dorsal root ganglion and 2 hours for the skin and spinal cord) and incubated in HBSS at 65–68 °C for 30 minutes to inhibit the endogenous alkaline phosphatase. Tissues were washed and incubated with NBT and BCIP to visualize the PLAP signals. The tissues were cleared in BABB (Benzyl Alcohol and Benzyl Benzoate, 1:2 mixed together) before imaging on a ZEISS SteREO Discovery V12 stereomicroscope with a color camera.

### Immunohistochemistry Staining

Immunohistochemistry staining was performed as previously described (Xing et al, 2021). The following antibodies were used: rabbit anti-MrgprC11 (custom-made by Proteintech groups, validated by a previous study, 1:500) (Han et al, 2018), chicken anti-GFP (AVES), rabbit anti- Protein Gene Product 9.5 (Abcam ab108986).

### Optogenetics Analysis

Two to five-month-old *MrgprC11*$^{ChR2}$ mice were used for the optogenetic analysis. We generated ChR2 homozygous mice for this assay since ChR2 heterozygous mice did not show significant behavioral responses after light stimulation. 473 nm blue light laser (Shanghai Laser and Optics Century, Blue Diode Laser) is guided through a 0.2 mm-diameter optical fiber and the tip of the fiber was placed 2–5 mm away from the skin. Ten trains of 10 Hz pulses with different powers (0.1–10 mW) were applied to the shaved trunk skin (T6–T10) or the glabrous skin with a cutoff time of 10 seconds to avoid non-specific behavior effects induced by laser heat. Laser power applied to the skin was measured at the tip of the optical fiber using a power meter.

### qPCR of Skin-Innervating Neurons

Skin-innervating neurons were labeled by injection of neuronal tracer CTB-555 (Cholera Toxin Subunit B conjugated with Alexa Fluor 555, red color) into the skin of *MrgprC11*$^{ChR2}$ mice. Dorsal root ganglia innervating the injected area were collected and dissociated 10 days after the injection. MrgprC11$^{+}$ skin-innervating neurons labeled by both ChR2-H134R-EYFP and CTB-555 were collected using FACS sorting and first strand cDNA was synthesized using Invitrogen Cells-to-cDNA™ II Kit (AM1723). Quantitative RT-PCR was performed using a StepOnePlus RT-PCR System (Thermo Fisher Scientific) with the SYBR Green detection method. The CT values were analyzed by the $2^{-\Delta CT}$ method to determine the normalized expression ratio of target genes. Primer sequence:ChR2-Forward: GTCGGAC GCGAACTTTTGTTChR2-Reverse: ACC ATTTCAATGGCGCACAC

### Behavioral Analysis

All experiments were performed with an experimenter blind to genotype using protocols approved by the Animal Care and Use Committee of Georgia Institute of Technology School of Biology. All behavior tests were performed from 8:00 AM to 1:00 PM in the light cycle in our animal facility. All mice were acclimated for 30–60 minutes to their testing environment the day before the behavioral tests. To evaluate scratching behavior, 50 μl Bam8-22 (Genscript) was injected into the nape of the neck or the thoracic back skin. To evaluate glabrous skin itch behavior, 4 μl Bam8-22 was injected into the center of the planter hind paw using a custom-made 10 μl Hamilton syringe with a 30 gauge needle. The behavioral responses were recorded and quantified. The glabrous skin biting behavior was quantified in slow motion (0.25× normal speed).

## SUPPLEMENTARY REFERENCES

Han L, Limjunyawong N, Ru F, Li Z, Hall OJ, Steele H, et al. Mrgprs on vagal sensory neurons contribute to bronchoconstriction and airway hyper-responsiveness. Nat Neurosci 2018;21:324–8.

Liu Q, Vrontou S, Rice FL, Zylka MJ, Dong X, Anderson DJ. Molecular genetic visualization of a rare subset of unmyelinated sensory neurons that may detect gentle touch. Nat Neurosci 2007;10:946–8.

Xing Y, Steele HR, Hilley HB, Zhu Y, Lawson K, Niehoff T, et al. Visualizing the itch-sensing skin arbors. J Invest Dermatol 2021;141:1308–16.

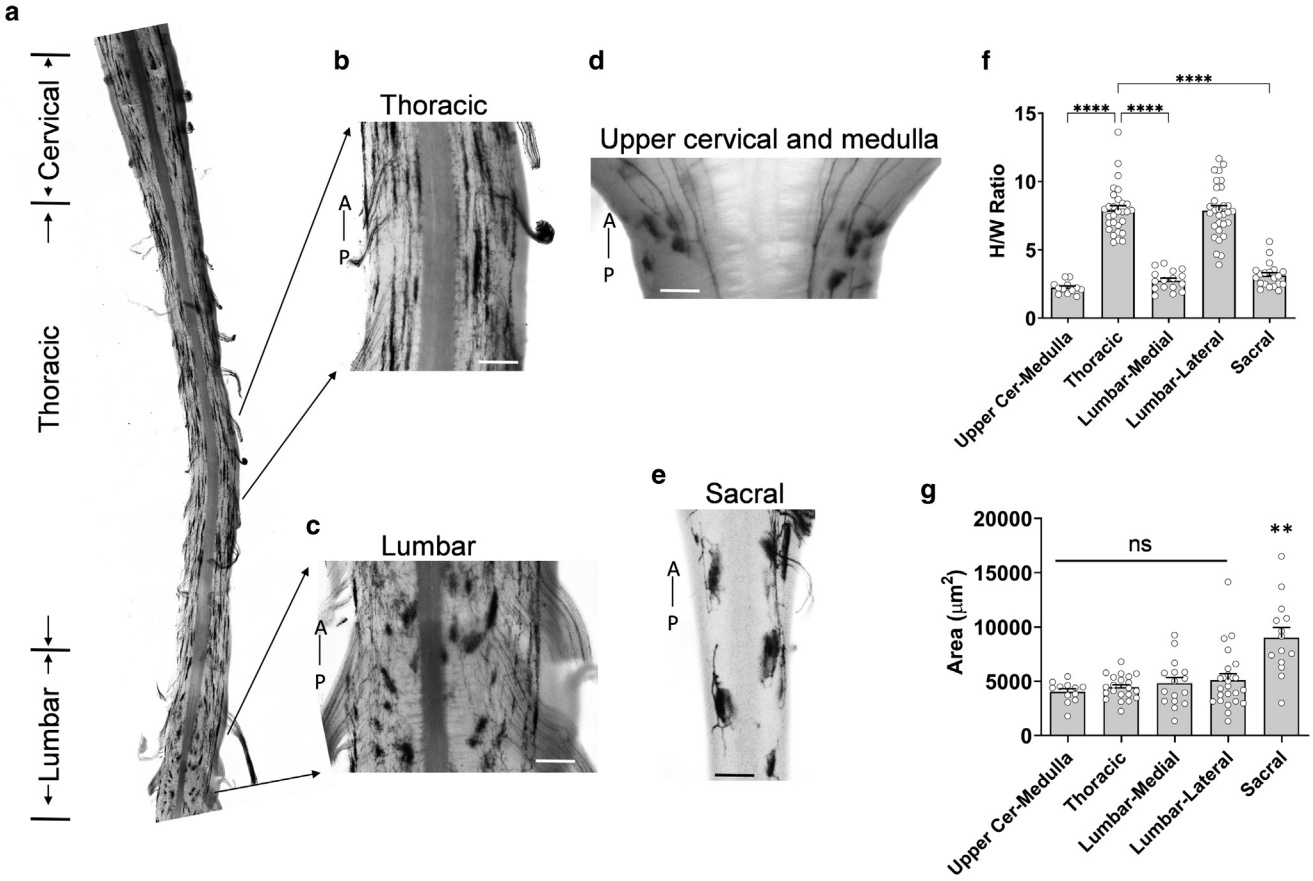


**Supplementary Figure S1. MrgprC11$^{+}$ central arbors exhibit regionally distinct morphology.** (**a**) Whole-mount PLAP histochemistry of a spinal cord from *MrgprC11$^{IAP}$* mice without tamoxifen treatment. (**b**–**c**) Part of the thoracic (**b**) and lumbar (**c**) spinal segments in **a** are shown in higher magnification. All MrgprC11$^{+}$ central arbors in the thoracic segments exhibit long morphology with rostrocaudal elongation and mediolateral compression. MrgprC11$^{+}$ central arbors in the lateral lumbar segments exhibit long morphology, whereas arbors in the medial lumbar segments show round morphology. (**d**) All MrgprC11$^{+}$ central arbors in the upper cervical and medulla regions exhibit round morphology. (**e**) All MrgprC11$^{+}$ central arbors in the sacral spinal segments exhibit round morphology and are larger than arbors in other regions. (**f**–**g**) Quantification of the Height/Width ratio (**f**) and arbor area (**g**). Arbors from 5 mice were analyzed. Data are represented as mean ± SEM. One-way ANOVA for **f**–**g**. $^{**}P < .01$. $^{***}P < .005$. $^{****}P < .001$. A, anterior; ns, not significant; P, posterior.